energy&fuels

Article

pubs.acs.org/EF

Steam Gasification Rates of Three Bituminous Coal Chars in an Entrained-Flow Reactor at Pressurized Conditions

Aaron D. Lewis, Troy M. Holland, Nathaniel R. Marchant, Emmett G. Fletcher, Daniel J. Henley, Eric G. Fuller, and Thomas H. Fletcher*

Department of Chemical Engineering, Brigham Young University, Provo, Utah 84602, United States

ABSTRACT: Three bituminous coal chars (Illinois #6, Utah Skyline, and Pittsburgh #8) were gasified separately at total pressures of 10 and 15 atm in an entrained-flow reactor using gas temperatures up to 1830 K and particle residence times <240 ms. Most of the experiments were performed at conditions where the majority of particle mass release was due to H_2O gasification, although select experiments were performed at conditions where significant mass release was due to gasification by both H_2O and CO_2. The measured coal data were fit to three char gasification models including a simple first-order global model, as well as the CCK^N and CCK models that stem from the CBK model. The optimal kinetic parameters for each of the three models are reported, and the steam reactivity of the coal chars at the studied conditions is as follows: Pittsburgh #8 > Utah Skyline > Illinois #6.

1. INTRODUCTION

Gasification is the process by which any carbonaceous species can be converted through heterogeneous reaction into a gaseous fuel termed *synthesis gas* (or *syngas*) that is mainly composed of H_2 and CO. Char gasification is preceded by devolatilization and usually takes place at high temperatures and pressures to speed along the relatively slow rates of the char gasification reactions. Coal is the leading feedstock in commercial gasification, and the uses of syngas produced from commercial gasifiers include chemical production (45%), liquid transportation fuels (38%), power (11%), and gaseous fuels (6%).[1]

Entrained-flow gasifiers are the most widely used industrial reactors to gasify coal commercially.[2,3] One advantage of this type of gasifier is that it allows the highest throughput per reactor volume. Entrained-flow gasifiers convert pulverized particles, and use high temperature (1200−2000 °C) and pressure (4−65 atm) to ensure high carbon conversion in the time frame of a few seconds.[2−4] Pulverized particles in commercial entrained-flow reactors experience high initial heating rates, which are reported as high as 10^6 K/s.[5,6]

Measuring the rates at which char gasifies is of interest, since char conversion is the rate-controlling step in a gasifier; the faster steps of drying, pyrolysis, and volatiles combustion occur much more quickly in the gasification of a solid fuel. Table 1 contains a summary of recent experiments from the literature that involved H_2O gasification rates of coal char, along with some entrained flow CO_2 gasification experiments. Since pyrolysis conditions are known to affect the gasification reactivity of coal char,[7−10] information regarding the conditions at which the chars were generated is located in separate columns in the table than the conditions at which the chars were gasified. The summary table prepared by Shurtz and Fletcher[11] is another good source of coal gasification rate studies. The vast majority of reported coal gasification rates have been measured using thermogravimetric analyzers (TGAs) at relatively low temperatures, pressures, and heating rates even though these conditions do not closely match the reaction conditions of industrial entrained-flow gasifiers. Only a few research groups have attempted to investigate char gasification rates at the experimentally challenging conditions of high heating rate and high temperature typical of entrained-flow gasifiers. This study includes the measurement of H_2O gasification rates of three pulverized coal chars in entrained flow using a high-pressure flat-flame burner (HPFFB) reactor at conditions of high pressure (10−15 atm), temperature ($T_{gas,max}$ > 1600 K), and initial particle heating rates (~10^5 K/s). The measured rates are especially meaningful, since it is known that the initial particle heating rate and pressure affect the pore structure and morphology of the char.[12] The measured char gasification data were fit to three different models, and the optimal kinetic parameters are reported.

The char gasification rates reported in this work allow a prediction of char conversion for pulverized particles in entrained-flow conditions. Therefore, the gasification rates can be used in CFD codes by accounting for the exchange of gas species and enthalpy between the char particles and the gas phase.[11] The insight gained into fuel reactivity will also be of value in the determination of optimal dimensions of future entrained-flow gasifiers, where high char conversions are desired in short residence times, and where any overdesign of the gasifier results in substantial capital equipment costs.

The reported char gasification rates in this work can also aid in the optimal operation of commercial entrained-flow gasifiers.[2] For example, a substoichiometric amount of oxygen is supplied to a gasifier to react with the fuel, since the exothermic combustion reaction provides the heat necessary to drive the endothermic gasification reactions. Although operating the gasifier at an increased O_2/fuel ratio raises the gasifier temperature, the syngas is then composed of a higher

Received: November 20, 2014
Revised: February 17, 2015
Published: February 17, 2015

DOI: 10.1021/ef502608y
Energy Fuels 2015, 29, 1479−1493

Table 1. Recent Coal H_2O Gasification Kinetic Studies

source	pyrolysis apparatus, particle size, and heating rate	pyrolysis temperature and pressure	gasification reactor, reactant(s), sample size; particle size	gasification temperature and total pressure
Weeda et al.[13]	entrained flow reactor	1100 °C	thermo balance	813−925 °C
	106−150 μm	1.4 s	H_2O, H_2	<1.2 MPa
	10^4 °C/s	not specified	30 mg	
Ahn et al.[14]	pressurized drop-tube furnace	1400 °C	pressurized drop-tube furnace	900−1400 °C
	45−64 μm	0.6 s	CO_2	0.5−1.5 MPa
	10^4 °C/s	0.101 MPa	not specified	
Kajitani et al.[15]	drop-tube furnace	1400 °C	pressurized drop-tube furnace	1100−1500 °C
	10−100 μm	3 s	CO_2, H_2O	0.2−2 MPa
	not specified	0.101 MPa	not specified	
Kajitani et al.[16]	drop-tube furnace	1397 °C	pressurized drop-tube furnace and TGA	1000−1400 °C
	∼40 μm	3 s	CO_2	1−3 MPa
	not specified	not specified	not specified	
Fermoso et al. 2010[17]	fixed-bed reactor	1100 °C	TGA	727−1127 °C
	1−2 mm	30 min	H_2O	0.101 MPa
	15 °C/min	0.101 MPa	5 mg; <150 μm	
Huang et al. 2010[18]	fluidized-bed reactor	840 °C	TGA	850−950 °C
	pulverized particles	20 min	CO_2, H_2O	0.101 MPa
	1000 °C/s	0.101 MPa	10 mg; <200 μm	
Liu et al. 2010[19]	fluidized bed (*in situ*)	1000−1500 °C	fluidized bed	1000−1500 °C
	177−210 μm	up to 10 min	H_2O	0.101 MPa
	rapid heating rate	0.101 MPa	177−210 μm	
Fermoso et al. 2011[7]	fixed-bed reactor	800−1000 °C	TGA	850−1050 °C
	75−150 μm	0.101−2.03 MPa	H_2O	0.101 MPa
	5000 °C/s		5 mg; 75−150 μm	
Xu et al. 2011[20]	electric oven	900 °C	tube reactor in oven	850−950 °C
	6 × 10 mm pellets	7 min	H_2O	0.101 MPa
	heat rate not given	0.101 MPa	1 g; 6 × 10 mm pellets and pulverized sizes	
Li et al. 2012[21]	TGA	900−1100 °C	TGA	900−1100 °C
	particle size not given	*in situ* pyrolysis	CO_2, H_2O	0.101 MPa
	10 °C/min	0.101 MPa	15−20 mg	
Fan et al. 2013[22]	tube furnace	900 °C	TGA	850−1050 °C
	0.5−1 mm	5 min	CO_2, H_2O	0.101 MPa
	heat rate not given	0.101 MPa	15 mg; 0.5−0.8 mm	
Ren et al. 2013[4]	DIFBR[a]	1000−1600 °C	DIFBR[a]	1000−1600 °C
	2−4 mm single particle	in situ pyrolysis	CO_2, H_2O	0.101 MPa
	∼490−790 °C/s	0.101 MPa	50 ± 1 mg particle	
Tremel and Spliethoff 2013[23]	entrained-flow reactor	1200−1600 °C	HPTGA[b]	600−1000 °C
	particle size not given	1.3−1.7 s	CO_2, H_2O	0.5, 1.0, 2.5 MPa
	10^4−10^5 °C/s	0.5, 2.5 MPa	40−60 mg; >42 μm	
Huo et al. 2014[24]	fixed-bed reactor	850 °C	TGA	850−1300 °C
	<40, 100, 250, 500 μm	30 min	CO_2, H_2O	0.101 MPa
	25 °C/min	0.101 MPa	5 mg	
Yan et al. 2014[25]	fixed-bed reactor	900 °C	PFBDR[c]	950 °C
	particle size not given	30 min	H_2O	0.1, 1.0, 2.0 MPa
	150 °C/s	likely 0.101 MPa	20 mg	
Bai et al. 2014[26]	apparatus not specified	800−1100 °C	TGA	750−1100 °C
	<125 μm	30 min	CO_2, H_2O, CO_2 + H_2O	0.101 MPa
	10 °C/min	0.101 MPa	∼15 mg; <125 μm	

[a]Drop-in fixed-bed reactor. [b]High-pressure TGA. [c]Pressurized fixed-bed differential reactor.

Table 2. Results of the Ultimate and Proximate Analyses of 45−75 μm Raw Coals

sample	apparent density (g/cm^3)	moisture (wt %, as recd)	ash (wt %, dry)	volatiles (wt %, daf[a])	C (wt %, daf)	H (wt %, daf)	N (wt %, daf)	O[b] (wt %, daf)	S (wt %, daf)
ILL #6	1.25	3.45	8.49	43.37	75.09	5.21	1.34	14.02	4.35
Utah	1.25	2.41	7.87	47.06	77.39	5.57	1.57	14.87	0.61
Pitt #8	1.31	1.67	12.41	37.73	80.86	5.39	1.64	10.61	1.49

[a]daf = dry and ash-free basis. [b]Calculated by difference.

DOI: 10.1021/ef502608y
Energy Fuels 2015, 29, 1479−1493

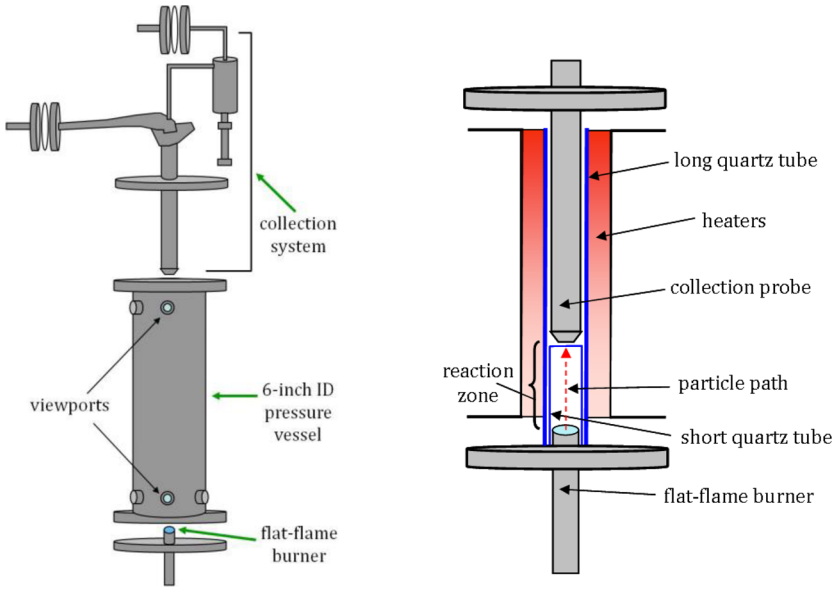

Figure 1. External and cutaway views of BYU's HPFFB reactor.

concentration of undesired CO_2 and H_2O. Conversely, operating the gasifier at a decreased O_2/fuel ratio results in a higher concentration of desired product gases (i.e., CO and H_2), but the gasifier temperature will decrease which may result in incomplete char conversion in the limited residence time available in the entrained-flow gasifier. Therefore, char gasification rates provide valuable insight into the most favorable operating conditions of a gasifier.

2. EXPERIMENTAL SECTION

2.1. Sample and Apparatus. Three bituminous coals (Illinois #6, Utah Skyline, and Pittsburgh #8) were used in the steam char gasification experiments in this work. The abbreviated names of ILL #6, Utah, and Pitt #8 will be used to refer to these coals, respectively. Table 2 includes the results of the ultimate and proximate analyses of the three raw coals, in addition to measured particle apparent densities.

The char gasification experiments in this research were conducted at entrained-flow conditions using the high-pressure flat-flame burner reactor (see Figure 1). The HPFFB reactor well approximated the reaction conditions characteristic of industrial entrained-flow gasifiers by allowing pulverized particles that experienced rapid initial particle heating rates to react in entrained flow at high temperatures and pressures for short times (<1 s). The HPFFB used a Hencken burner as the sole heat source of the reactor, since heaters were not utilized in this study. The burner is approximately 25 mm in diameter and used about 100 small-diameter tubes (0.61 mm ID) to create numerous diffusion flamelets by feeding gaseous fuel through the tubes and introducing oxidizer gas in between the fuel tubes. The multitude of individual flamelets created a flat flame less than 1 mm thick above the burner, thus enabling well characterized reactor conditions at which coal chars were gasified.

Particles were entrained in nitrogen and carried to the middle of the burner face through a small metal tube (1.346 mm ID) at a rate less than 2 g/h. Upon exiting the feed tube, the coal particles reacted in laminar flow while traveling upward through a circular quartz tube (26 mm ID) in an environment determined by postflame gas composition. A water-cooled collection probe was used to quench the reacting particle by quickly lowering the temperature and also by using high flow rates of nitrogen. A virtual impactor and cyclone in the collection system separated the char aerodynamically from the exhaust and quench gases, while any tar/soot collected on water-cooled glass fiber filters.

Gas temperature was controlled in the HPFFB by adjusting gas flow rates to the burner, which changed the stoichiometry. The HPFFB centerline gas temperature profiles were measured using a 422 μm diameter B-type thermocouple corrected for radiation losses;[27] the gas temperature correction in the near-burner region was approximately 85 K for the conditions used in this study. The particle residence time in the char gasification experiments was manipulated primarily by adjusting the distance between the burner and collection probe. Additional details concerning the HPFFB reactor have been reported elsewhere.[11,27−30]

2.2. Reinjection Strategy. Fully pyrolyzed coal char generated at pressurized and high-heating-rate conditions was fed in the HPFFB reactor during coal gasification experiments at a rate less than 0.2 g/h to prevent clogging and to represent single particle behavior. It would have been ideal to conduct char gasification experiments following *in situ* pyrolysis like what occurs in commercial entrained-flow gasifiers, but soot contamination of the char prevented this. A good mass balance for an experimental run (using weights of fed and collected material) is interrupted when a significant amount of soot contaminates the char, since it is experimentally challenging to separate the soot from the char[29] and assign accurate mass fractions to each. Soot-laden char also prevents accurate mass release values from being calculated when ash is assumed to act as a tracer. Hence, the method of reinjecting fully pyrolyzed coal char to measure rates of char conversion was pursued, in a manner similar to other researchers.[11,31,32] Hurt et al.[31] reported that capture and reinjection of coal char had little effect on the measured reactivity from data taken when feeding Illinois #6 coal through an entrained-flow reactor. It is therefore assumed that the measured char gasification data from the current study are applicable to industrial entrained-flow processes where char gasification typically follows *in situ* pyrolysis.

The coal chars used in the HPFFB gasification experiments were generated by feeding raw, sized (45−75 μm) coals in the HPFFB reactor at the same total pressure that the chars would later be reinjected. The char-generation conditions had peak gas temperatures near 1850 K and utilized a 19 mm collection height (~40 ms). About 2 mol % O_2 was used in the postflame environment in order to oxidize the tar before soot could be formed. The generated coal chars from the three total pressures (10, 12.5, and 15 atm) were sieved, and the size fraction used during char gasification reinjection experiments was determined solely by which size fraction contained the highest yields of particles. The Utah Skyline steam gasification experiments used the 45−75 μm fraction, while both the Illinois #6 and Pittsburgh #8 steam experiments utilized the 75−106 μm fraction. The increased quantities of the 75−106 μm fraction are evidence that char swelling during high-

DOI: 10.1021/ef502608y
Energy Fuels 2015, 29, 1479−1493

Table 3. Matrix of HPFFB Experiments for Char Gasification Tests by Steam

total pressure	max gas temperature	equilibrium H_2O, CO_2, CO, N_2	reference residence time	coal sample	gasification residence times
10 atm	1814 K	7.5, 14.2, 1.9, 75.7 mol %	42 ms	Utah	107; 183 ms
			45 ms	Pitt #8	116; 199 ms
			45 ms	ILL #6	116; 198 ms
12.5 atm	1782 K	7.7, 14.1, 2.3, 75.1 mol %	47 ms	Utah	118; 202 ms
			52 ms	Pitt #8	135; 232 ms
			52 ms	ILL #6	134; 231 ms
15 atm	1611 K	7.3, 11.4, 2.8, 77.5 mol %	55 ms	Utah	139 ms
			59 ms	Pitt #8	153 ms
			59 ms	ILL #6	153 ms
15 atm	1830 K	8.6, 13.7, 2.5, 74.4 mol %	49 ms	Utah	126; 219 ms
			52 ms	Pitt #8	135; 237 ms
			51 ms	ILL #6	135; 236 ms

heating-rate pyrolysis (up to 6.7×10^4 K/s) had a greater effect on the Illinois #6 and Pittsburgh #8 coals than the Utah Skyline coal, since 45−75 μm raw coal was fed during the generation of all three pyrolyzed chars. Shurtz[29,33] discusses the effect of initial particle heating rate on coal char swelling in more detail. The chosen size fractions of fuel char (45−75 or 75−106 μm) for HPFFB gasification experiments were used to simulate pulverized coal sizes used commercially but also allowed particle temperature gradients to be ignored in modeling.

2.3. Particle Mass Release. The equations most commonly used to calculate particle mass release on a dry, ash-free (daf) basis in entrained-flow experiments from a mass balance and ash-tracer respectively are

$$\%\ \mathrm{MR\ (daf)} = \left(\frac{m^0_{\mathrm{fed}} - m_{\mathrm{char\ collected}}}{m^0_{\mathrm{fed}} - m^0_{\mathrm{ash,fed}}} \right) \times 100 \quad (1)$$

$$\%\ \mathrm{MR\ (daf)} = \left(\frac{1 - \frac{x^0_{\mathrm{ash,fed}}}{x_{\mathrm{ash,char\ collected}}}}{1 - x^0_{\mathrm{ash,fed}}} \right) \times 100 \quad (2)$$

Since a char reinjection approach was utilized in this study, m^0_{fed} is the dry mass of coal char fed, $m_{\mathrm{char\ collected}}$ is the dried mass of partially gasified char collected after an experiment, and $m^0_{\mathrm{ash,fed}}$ is the dry mass of ash in the fed feedstock. The mass fraction of ash (dry basis) in the char fed is $x^0_{\mathrm{ash,fed}}$, whereas $x_{\mathrm{ash,char\ collected}}$ is defined as the mass fraction of ash (dry basis) in the collected char.

Equation 2 does not depend on collection efficiency, and allows accurate particle mass release to be calculated (assuming that original ash remains with the char) even if a good mass balance is disturbed by spills, feeding-line clogs, or incomplete documentation of weight measurements of the fed material and collected char. Both eqs 1 and 2 assume that ash remains with the particle during a char gasification experiment. If ash from the particle is released to the gas phase during an experiment, eqs 1 and 2 will overestimate and underestimate the particle daf mass release, respectively. The numerator in eq 1 reflects the organic mass that is evolved *if* all the ash remains with the particle. However, when ash is released from the particle, the numerator in eq 1 reflects the mass of ash that was liberated in combination with the organic mass release due to char conversion. Equation 3 was derived to calculate accurate particle mass release on a daf basis even when ash is released from the particle during an experiment. The numerator in the equation represents the organic mass of the particle that was converted:

$$\%\ \mathrm{MR\ (daf)} = \left(\frac{m^0_{\mathrm{char,fed}}(1 - x^0_{\mathrm{ash,fed}}) - m_{\mathrm{char\ collected}}(1 - x_{\mathrm{ash,char}})}{m^0_{\mathrm{char,fed}} - m^0_{\mathrm{ash,fed}}} \right) \times 100 \quad (3)$$

Note that accurate mass release values by eq 3 are dependent upon a good mass balance, which is regularly attained in the HPFFB reactor. For example, the collection efficiency of the HPFFB reactor was measured to be 98.0% using collection heights in the range 76−241 mm.[27,34] Additionally, the best possible mass balance was ensured by cleaning out the collection system after each experiment to most accurately assign weights of material fed and collected.

Particle mass release calculated by eq 3 was the primary value used in the char gasification modeling of this study, even though ash-tracer mass release values (see eq 2) were also considered. Ash often was liberated from the bituminous coal chars during experiments, as determined using a mass balance of the ash. Shurtz[29] also observed ash liberation from coals fed at high initial particle heating rates, and documented that plotting the daf particle mass release values by the ash-tracer method in eq 2 resulted in "very noisy trends". However, using eq 3 to calculate particle mass release values resolved this issue.

2.4. Test Matrix and Experimental Details. Two different sets of gas conditions were used in the coal char gasification experiments in the HPFFB reactor. The first set of gas conditions was used to measure particle mass release at total pressures of 10, 12.5, and 15 atm for Illinois #6, Utah Skyline, and Pittsburgh #8 coal chars at conditions where the char conversion was primarily due to *steam* gasification. This first set of gas conditions will be referred to as the *steam conditions* in this work. Gasification by CO_2 accounted for some particle mass release when coal char was fed at the first set of gas conditions, since it was not possible to have postflame reaction environments completely absent of CO_2 in the HPFFB reactor. However, the char mass release caused by CO_2 was accounted for in the char gasification modeling. The second set of HPFFB gas conditions was used to study the gasification of a single coal char (Illinois #6) at a total pressure of 15 atm using conditions where significant char conversion (i.e., ≥17 wt % daf char basis) was attributed separately to steam *and* CO_2. The second set of gas conditions will be referred to as the *steam/CO_2 conditions* in this work.

The matrix of coal char HPFFB gasification experiments for the first and second set of gas conditions is included in Tables 3 and 4,

Table 4. Matrix of HPFFB Experiments for Char Gasification Tests by Steam/CO_2 When Feeding 75−106 μm Illinois #6 Char

total pressure	max gas temperature	equilibrium H_2O, CO_2, CO, N_2	reference residence time	gasification residence times
15 atm	1812 K	7.7, 83.2, 7.9, 1.1	51 ms	130, 222 ms
15 atm	1879 K	7.5, 33.3, 10.5, 47.7	49 ms	130, 224 ms

respectively. Also included in the tables are details about the gas conditions including total pressure, maximum measured centerline gas temperature, and equilibrium composition of the postflame HPFFB environments as calculated by thermodynamic equilibrium. The HPFFB gas conditions in this work are identified by the total pressure and maximum measured centerline gas temperature of a particular condition. Table 5 provides a summary of the properties of all the fuel

DOI: 10.1021/ef502608y
Energy Fuels 2015, 29, 1479−1493

Table 5. Properties of Coal Fuel Chars Used in HPFFB Gasification Experiments

condition at which fuel char was fed	feedstock	pyrolysis and gasification pressure (atm)	ash (wt %, dry)	sieved size (μm)	mass mean (μm)	apparent density (g/cm^3)
steam[a]	Utah	10	27.8	45−75	61.7	0.242
10 atm; $T_{gas,max}$ = 1814 K	Pitt #8	10	10.6	75−106	85.9	0.161
	ILL #6	10	12.1	75−106	84.5	0.145
steam[a]	Utah	12.5	24.8	45−75	62.7	0.203
12.5 atm; $T_{gas,max}$ = 1782 K	Pitt #8	12.5	9.4	75−106	86.0	0.170
	ILL #6	12.5	15.6	75−106	89.3	0.145
steam[a]	Utah	15	23.6	45−75	68.6	0.186
15 atm; $T_{gas,max}$ = 1611 and 1830 K	Pitt #8	15	10.0	75−106	82.3	0.154
	ILL #6	15	13.9	75−106	78.2	0.144
steam/CO_2[b]	ILL #6	15	12.9	75−106	86.3	0.144
15 atm; $T_{gas,max}$ = 1812 and 1879 K						

[a]Contains some CO_2; see Table 3. [b]See Table 4.

chars used in the HPFFB gasification experiments. Surface area measurements of select fuel char samples have been documented elsewhere.[27]

One additional HPFFB gas condition used in this study that is not summarized in Table 3 or Table 4 had a total pressure of 10 atm and a peak gas temperature of 1850 K. This extra condition essentially did not contain steam and was used to aid in the accounting of char conversion due to CO_2 gasification when coal char was fed at the HPFFB steam conditions (see Table 3). The equilibrium postflame CO_2, H_2O, CO, and N_2 concentrations of the 10 atm $T_{gas,max}$ = 1850 K nonsteam condition were 20.8, 0.9, 7.7, and 70.0 mol %, respectively. Additional details of this gas condition have been documented elsewhere.[27]

Particle mass release was typically measured at three residence times per gas condition at collection heights of 25, 76, and 127 mm above the burner. The first collection height at 25 mm above the burner served as a reference data point, since only the particle mass release after this first data point was used in the modeling. The particle residence time of this first sample location is shown as the "reference residence time" in Tables 3 and 4. Only two residence times were tested at the 15 atm $T_{gas,max}$ = 1611 K condition (see Table 3), since water condensation negatively affected particle feeding when collection heights greater than 76 mm were attempted at this relatively cool condition.

A high-speed camera (125 frames/s) was used to measure particle velocities through the bottom viewport of the HPFFB reactor (see Figure 1) to aid in the calculation of particle residence times.[27] The particle velocity profiles of Utah Skyline chars at the HPFFB steam conditions (see Table 3) are shown in Figure 2. Note that the particle velocities were not constant at the nonisothermal gas conditions of the HPFFB reactor. However, the nonuniform particle velocity profile was taken into account in the calculation of all particle residence times in this study.

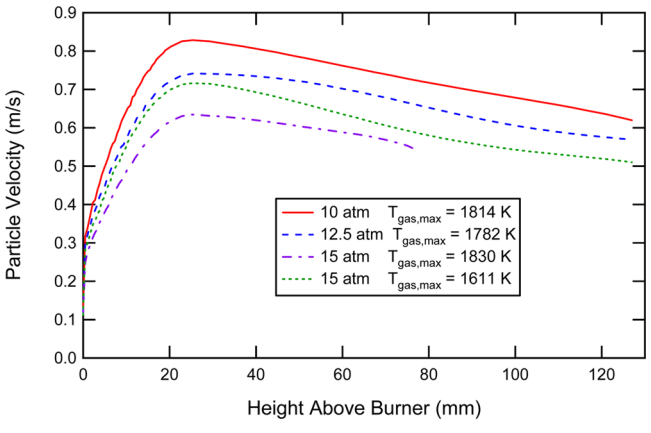

Figure 2. Particle velocity profiles of 45−75 μm Utah Skyline chars at steam conditions in the HPFFB reactor.

The steam concentrations used in this study were limited to less than 9 mol % in the postflame environment (see Tables 3 and 4) due to concerns about damaging the burner head. Supplying extra H_2 to the burner resulted in higher concentrations of steam in the postflame environment but also caused the flame to "sit" closer to the burner surface due to the high flame speed of H_2. Supplying the burner with excessive amounts of H_2 can greatly reduce the life of the burner, thus explaining why only conservative amounts of H_2 were used in this study.

The measured particle mass release HPFFB data from the char gasification experiments are summarized in Tables 6 and 7. Replicate HPFFB char gasification experiments were performed at about 30% of the conditions, and the repeated mass release measurements were typically within 4 wt % daf of the previously measured values. Additional details and results of the HPFFB experiments are available elsewhere.[27]

3. MODELING OF CHAR GASIFICATION DATA BY A FIRST-ORDER MODEL

The coal char gasification data measured from the HPFFB reactor were first used to regress kinetic coefficients to a relatively simple global first-order model, although the data were also used to fit parameters to the char conversion kinetics (CCK) model and its *n*th-order variant named the CCK^N model.[11,29]

3.1. Modeling of Gasification Data from the HPFFB Steam Conditions. Kinetic parameters were first fit to the global first-order model[28,35−37] using measured data from the HPFFB steam conditions (see Table 3). The char conversion rate (r''_p) in this empirical model is normalized by particle external surface area, and is a function of particle temperature, partial pressure of reactant gas at the particle surface, external particle surface area, and time

$$r''_p = \frac{1}{A_p}\frac{dm_p}{dt} = -k_{rxn}P_{reactant,surf} = -\left[A\exp\left(\frac{-E}{RT_p}\right)\right]P_{reactant,surf} \quad (4)$$

where A_p is the external surface area of the spherical particle ($4\pi r^2$), m_p is the particle mass, t is the time, k_{rxn} is the gasification rate constant, $P_{reactant,surf}$ is the partial pressure of CO_2 or H_2O at the particle surface, E is the activation energy, A

DOI: 10.1021/ef502608y
Energy Fuels 2015, 29, 1479−1493

Table 6. Summary of Averaged Particle Mass Release Data at the HPFFB Steam Conditions

total pressure	max gas temperature	equilibrium H_2O; CO_2	Utah res. time	Utah %MR[a] (daf)	Pitt #8 res. time	Pitt #8 %MR[a] (daf)	ILL #6 res. time	ILL #6 %MR[a] (daf)
10 atm	1814 K	7.5; 14.2 mol %	42 ms	17.7	45 ms	11.6	45 ms	14.0
			107 ms	40.9	116 ms	26.2	116 ms	22.5
			183 ms	46.3	199 ms	40.1	198 ms	24.1
12.5 atm	1782 K	7.7; 14.1 mol %	47 ms	18.9	52 ms	17.1	52 ms	22.6
			118 ms	35.1	135 ms	38.8	134 ms	36.7
			202 ms	72.4	232 ms	60.6	231 ms	41.5
15 atm	1611 K	7.3; 11.4 mol %	55 ms	20.5	59 ms	10.2	59 ms	8.9
			139 ms	26.8	153 ms	18.5	153 ms	27.5
15 atm	1830 K	8.6; 13.7 mol %	49 ms	21.6	52 ms	10.2	51 ms	25.2
			126 ms	49.1	135 ms	44.8	135 ms	57.4
			219 ms	75.9	237 ms	68.7	236 ms	66.3

[a]Mass release on a daf char basis.

Table 7. Summary of Averaged Particle Mass Release Data at the HPFFB Steam/CO_2 Conditions when Feeding Illinois #6 Char

total pressure	max gas temperature	equilibrium H_2O; CO_2	residence time	%MR[a] (daf)
15 atm	1812 K	7.7; 83.2 mol %	51 ms	22.3
			130 ms	54.3
			222 ms	68.0
15 atm	1879 K	7.5; 33.3 mol %	49 ms	20.5
			130 ms	64.0
			224 ms	75.5

[a]Mass release on a daf char basis.

is the pre-exponential factor, T_p is the particle temperature, and R is the ideal gas constant. The reduction of A_p during conversion was taken into account using measured changes in particle diameter.[27] The kinetic parameters E and A for the first-order model in eq 4 were determined by minimizing the sum-squared error between measured and predicted particle mass release values from char gasification. The partial pressures of CO and H_2 were neglected in the first-order modeling, since the simple model did not contain any inhibitory mechanisms. However, the retarding influence of CO on the CO_2/char gasification reaction has been shown to have the most pronounced effect at conditions of lower temperatures and higher CO/CO_2 atomic ratios than those studied here.[38] Additional details about regressing optimal kinetic parameters for the first-order global gasification model have been documented.[28] Since only the gas temperature (T_{gas}) was measured, T_p was calculated from a particle energy balance at each time step

$$m_p C_p \frac{dT_p}{dt} = h_c A_p (T_{gas} - T_p) + \varepsilon_p \sigma A_p ({T_{surr}}^4 - {T_p}^4) + \frac{dm_p}{dt} \Delta H_{rxn} \quad (5)$$

where C_p is the particle heat capacity, h_c is the heat transfer coefficient ($Nu \cdot k_{gas}/d_p$), ε_p is the emissivity of the char particle, σ is the Stefan–Boltzmann constant, ΔH_{rxn} is the heat of reaction for the CO_2 or H_2O gasification, and T_{surr} is the surroundings temperature. The left-hand side of eq 5 was set equal to zero with the assumption that the particle temperature is near steady state with its surroundings when using time steps of approximately 0.15 ms. Although the first-order gasification model in eq 4 only implicitly accounts for any pore diffusion effects in the regressed kinetic parameters, mass transfer through the boundary layer of the particle is explicitly considered at each time step which allows calculation of $P_{reactant,surf}$.[27] Changes in gas composition over the length of the reactor due to particle conversion were ignored due to the low char feed rates (<0.2 g/h) used in the HPFFB gasification experiments.

Representative gas and particle temperature profiles are included in Figure 3 for the 10 atm-generated Pittsburgh #8 char (75–106 μm) fed at the 10 atm $T_{gas,max}$ = 1814 K steam condition of the HPFFB. The particle temperatures in the figure were calculated by eq 5. As previously stated, data gathered from the first collection height at 25 mm above the burner served as reference data, since only the mass that was released from the particles after this first collection point was used in the modeling. In this way, the regressed kinetic parameters were not affected by any uncertainties in temperature history in the near-burner region. Temperature profiles from the other conditions used in this study are reported elsewhere.[27]

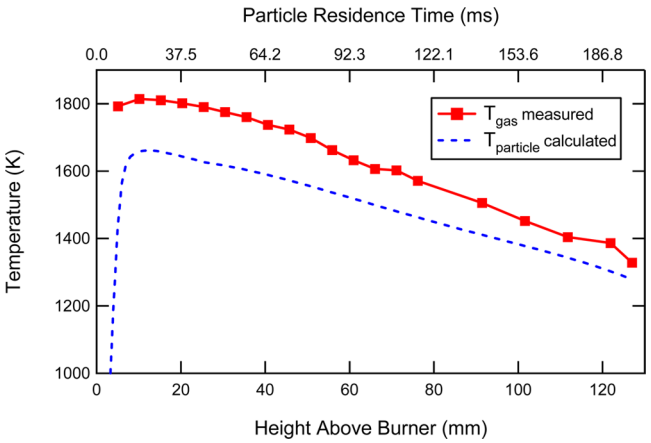

Figure 3. Measured centerline gas temperature profile and calculated particle temperature profile for Pittsburgh #8 coal char (75–106 μm) fed at the 10 atm $T_{gas,max}$ = 1814 K steam condition in the HPFFB reactor.

Kinetic parameters for the first-order model in eq 4 were regressed for all three coal chars using HPFFB data in Table 6, which was measured at conditions where the majority of char conversion was due to steam gasification. As described previously, the HPFFB steam conditions contained some

DOI: 10.1021/ef502608y
Energy Fuels 2015, 29, 1479–1493

CO_2, since it was not possible to have conditions completely free of CO_2 in the postflame environment of the reactor. Since the global first-order char conversion model is dependent on the partial pressure of a single gasification agent, it was therefore necessary to differentiate the measured particle mass release between that caused by CO_2 gasification and that due to H_2O gasification. To achieve this, particle mass release caused by CO_2 gasification in the HPFFB steam gasification experiments (see Table 3) was accounted for, and the remaining measured particle mass release was attributed to steam gasification. This approach assumed that char gasification rates by CO_2 and H_2O are additive, although researchers have not reached a common consensus about how to best model char gasification in mixed atmospheres of CO_2 and H_2O.[39,40] The particle mass release attributed to steam was then used to regress steam gasification kinetic parameters for the first-order model in eq 4.

The CO_2-induced particle mass release at the HPFFB steam conditions (see Table 3) was accounted for using published CO_2 coal char gasification rates,[11] or by using rates derived from mass release data collected at the HPFFB nonsteam condition (i.e., 10 atm $T_{gas,max}$ = 1850 K) described in section 2.4. The published char/CO_2 gasification rates of Shurtz and Fletcher[11] were convenient to use, since some of their reported rates involved the first-order model in eq 4. Their published coal char/CO_2 gasification rates from both measured data and empirical correlations were compared against the limited CO_2 gasification data collected from the 10 atm $T_{gas,max}$ = 1850 K nonsteam HPFFB condition, since this served as a quality check before their reported rates were used in this study.

The measured particle mass release at the 10 atm $T_{gas,max}$ = 1850 K nonsteam condition closely matched predictions from the work of Shurtz and Fletcher[11] for the Illinois #6 and Pittsburgh #8 chars. This provided confidence that their published CO_2 gasification rates properly accounted for the CO_2-induced particle mass release at the HPFFB steam condition for these two coal chars. The char/CO_2 gasification kinetic parameters for the Illinois #6 coal (i.e., A = 0.8876 g/cm^2/s/atm and E = 121.3 kJ/mol) came from Illinois #6 measured data by Shurtz and Fletcher,[11] whereas the parameters for the Pittsburgh #8 coal (i.e., A = 0.7772 g/cm^2/s/atm and E = 123 kJ/mol) came from their published correlation that was a function of the daf C/O mass ratio of the raw coal. However, the aforementioned correlation of Shurtz and Fletcher[11] which predicted kinetic constants for the first-order model in eq 4 did not yield accurate char/CO_2 gasification rates for the Utah Skyline char when compared to measured data from the 10 atm $T_{gas,max}$ = 1850 K nonsteam HPFFB condition. For example, the predicted char mass release was roughly double that which was measured (i.e., 59% vs 29% daf) when 45−75 μm Utah Skyline char was gasified for 285 ms (140 mm collection height). Therefore, to properly account for the CO_2-induced particle mass release of Utah Skyline char at the HPFFB steam conditions, CO_2 gasification kinetic parameters were regressed from the Utah Skyline data collected at the 10 atm $T_{gas,max}$ =1850 K nonsteam condition. The resulting A and E values were 1.0655 g/cm^2/s/atm and 121.3 kJ/mol, respectively. The E value was set to 121.3 kJ/mol in this case, since it was desired to make possible convenient reactivity comparisons with the Illinois #6 coal char, and allowing E to vary did not make significant improvements to the model fit when optimizing the CO_2 gasification kinetic parameters from the Utah Skyline nonsteam data set.

Figure 4 shows the particle mass release of Utah Skyline char caused by CO_2 and H_2O gasification after the first collection

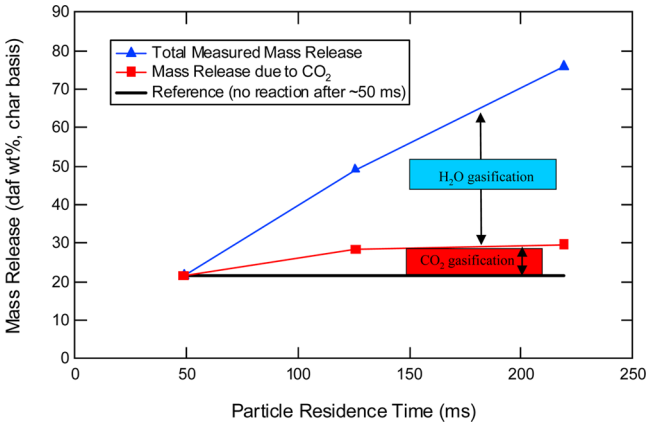

Figure 4. Effect of char mass release by H_2O and CO_2 gasification when feeding 15 atm-pyrolyzed 45−75 μm Utah Skyline char in the HPFFB reactor at the 15 atm $T_{gas,max}$ = 1830 K steam condition.

height at 25 mm above the burner at the 15 atm $T_{gas,max}$ = 1830 K steam condition. This figure shows that most of the coal char mass release measured at the HPFFB steam conditions was due to steam. Steam gasification in Figure 4 accounted for 85% of the particle mass release at the last collection point at a particle residence time of 219 ms. The 15 atm $T_{gas,max}$ = 1830 K steam HPFFB condition resulted in the highest char conversion by CO_2 of all four steam conditions, since it was the hottest condition and also because it contained the highest partial pressure of CO_2 and longest particle residence times. For a particular coal, the CO_2-induced particle mass release at the 15 atm $T_{gas,max}$ = 1830 K condition was the highest of any of the steam conditions (see Table 3). Hence, the Utah Skyline particle mass release caused by CO_2 in any of the other three steam conditions would be less than that shown in Figure 4.

In summary, particle mass release caused by CO_2 gasification in the HPFFB steam gasification experiments (see Table 3) was accounted for using the global first-order model in eq 4 (with CO_2 kinetic parameters from various sources), and the remaining measured particle mass release was attributed to steam gasification. The particle mass release data attributed to steam was then used to regress first-order steam gasification kinetic parameters for each coal char (ILL #6, Utah, Pitt #8) by minimizing the sum squared error between modeled and measured particle mass release data from four gas conditions in the HPFFB at typically three residence times per gas condition.

The regressed kinetic parameters are summarized in Table 8 but should be used with some caution. These values are predicted to yield satisfactory estimates of particle mass release caused by gasification of coal char for pulverized particle sizes similar to those used in this study (see Table 5). However, the first-order global model assumes no particle temperature gradients, which no longer applies when particle sizes are much beyond about 150−200 μm. In addition, large deviations from predicted mass release are known to occur at the latter stages of coal conversion.[31] Hence, the reported kinetic parameters in Table 8 are predicted to yield satisfactory estimates of char mass release due to *steam* gasification up to the measured conversions of 59, 68, and 64 wt % (daf char basis) for Illinois #6, Utah Skyline, and Pittsburgh #8 chars, respectively. Predictions of particle mass release at very high

DOI: 10.1021/ef502608y
Energy Fuels 2015, 29, 1479−1493

Table 8. H_2O and CO_2 Gasification Kinetic Parameters for Use in the Global First-Order Model

coal feedstock	E (kJ/mol)	A (H_2O gasification[a]) [(g carbon)/(cm²·s·atm H_2O)]	A (CO_2 gasification) [(g carbon)/(cm²·s·atm CO_2)]
Illinois #6	121.3[11]	5.35	0.89[11]
Utah Skyline	121.3	7.94	1.07[b]
Pittsburgh #8	123.0	12.55	0.78[11,c]

[a]The steam kinetic parameters were derived from data where T_p and $P_{H_2O,surf}$ values ranged from about 1250−1660 K and 0.65−1.25 atm, respectively. [b]This kinetic constant was derived in this project using limited data. [c]This kinetic constant was from a published empirical correlation based on elemental coal composition.

conversions require accounting for phenomena such as ash inhibition.[31]

It is important when reporting particle rates at high temperature to ensure that the measurements were not controlled entirely by film diffusion of reactant gas through the particle boundary layer. The maximum rate occurs under this scenario at high temperature when the concentration of reactant gas at the particle surface is approximately zero due to the rapid conversion at the particle surface. The chi factor, χ,[41,42] provides an indication of the effect of film diffusion on heterogeneous rates and was calculated for all the coal chars reacted in this work. The chi factor is defined as the measured rate divided by the maximum rate under film-diffusion control. The chi factor ranges from 0 to 1; film diffusion controls entirely when χ approaches unity, while the surface reaction controls when χ is much less than 1. The maximum χ value in the coal char gasification data sets was 0.06, indicating that the measured rates did not occur in the zone III regime[43] where film diffusion controls.

The parity plot shown in Figure 5 shows how the measured particle mass release data attributed to steam gasification

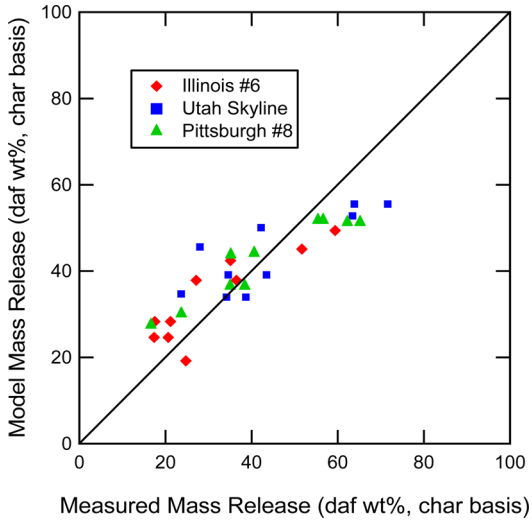

Figure 5. Fit with the first-order model using HPFFB particle mass release data attributed to H_2O gasification.

compared with that predicted by the first-order model using steam kinetic parameters in Table 8. The average absolute error using the following equation

$$\text{Absolute Error} = \frac{\sum_{i=1}^{n} |X_i^{M} - X_i^{E}|}{n} \quad (6)$$

was calculated for all the coal char data sets, where X_i^M and X_i^E are defined as the modeled and experimental particle mass release points, respectively. The absolute error between the Utah Skyline modeled and measured particle mass release data (daf char basis) was 8.5%. From similar calculations, the Illinois #6 and Pittsburgh #8 data had errors of 7.1 and 6.6%, respectively. The fits of the first-order model in Figure 5 are very encouraging considering the simplicity of the model.

When the reactivity data of two chars are fit to the same first-order model and they both use the same E value, convenient rate comparisons are performed by using ratios of pre-exponential factors. The steam kinetic parameters in Table 8 were derived from data where T_p and $P_{H_2O,surf}$ values ranged from about 1250−1660 K and 0.65−1.25 atm, respectively. Using data in this table reveals that Utah Skyline char is about 1.5 times (i.e., 7.94/5.35) more reactive to steam than the Illinois #6 char. Note in Table 8 the slightly higher activation energy for Pittsburgh #8 char that was used to stay consistent with the empirical correlation[11] used to model its CO_2 reactivity. However, when modeling the steam gasification data of Pittsburgh #8 char with E = 121.3, the corresponding optimal A value was 10.97. Using ratios of A values, this results in the Pittsburgh #8 char being 2.3 (i.e., 12.55/5.35) times more reactive to steam than Illinois #6 char and 1.6 (i.e., 12.55/7.94) times more reactive to steam than the Utah Skyline char at the measured conditions.

Note also in Table 8 that each coal char uses the same E value to model both its CO_2 and H_2O gasification rate. This allows rate comparisons of the CO_2 and H_2O gasification reactions of a given coal char using similar ratios of pre-exponential factors. Steam gasification rates of the coal chars were anywhere from 6 (i.e., 5.35/0.888) to 16 times (i.e., 12.55/0.777) faster than the corresponding CO_2 gasification rates. These rate comparison values between the steam and CO_2 gasification reactions are similar to those measured in a recent study by Huo et al.[24] at temperatures of 850 and 900 °C in a TGA reactor. For example, it was reported that the initial rates of steam gasification were about 6−13 and 4−10 times faster than CO_2 gasification of petroleum coke and anthracite coal chars, respectively.

3.2. Comparison to Reported First-Order Char Gasification Rates. The steam gasification rates of the three coal chars (Illinois #6, Utah Skyline, and Pittsburgh #8) from the current study were compared with published[11] CO_2 gasification rates of several different coals in Figure 6. Both the steam rates from the current study and the CO_2 rates from the literature were modeled using the same global first-order model in eq 4. The first-order rate constants in Figure 6 are each plotted over the particle temperature ranges of the experimental data used to regress the rate parameters. From the figure, it is seen that the steam gasification rates in this study exceeded the CO_2 gasification rates from the literature in every instance. This serves as a quality check of the steam gasification rates in the current work, since the H_2O gasification reaction has been reported in several instances[44−46] as being faster than the CO_2

DOI: 10.1021/ef502608y
Energy Fuels 2015, 29, 1479−1493

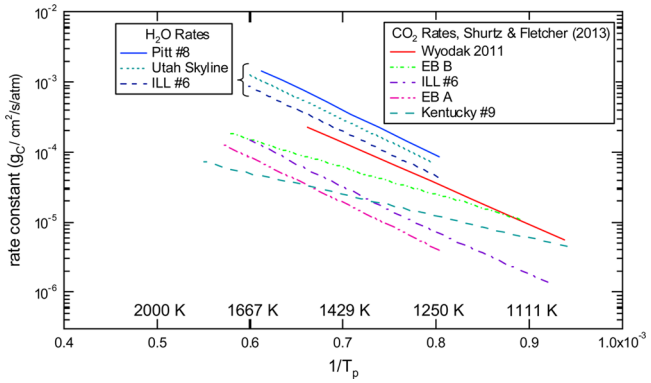

Figure 6. Comparison of the steam gasification rate constants of this work with the CO_2 gasification rate constants of Shurtz and Fletcher.[11] The coals EB A and EB B refer to Eastern Bituminous coals A and B, respectively.

gasification reaction (although reactivity differences between different coal chars should also be considered). Another quality check of the reported steam gasification rates is made possible, since Illinois #6 coal was common to both the current work and the published work.[11] The ratio of H_2O to CO_2 gasification rates for Illinois #6 coal char is 6, which is on the order of rate ratios reported in the literature for the H_2O and CO_2 gasification reactions.[8,22−24,45−48]

3.3. Modeling of Gasification Data from the HPFFB Steam/CO_2 Conditions. The combined steam and CO_2 experiments were modeled using first-order reactions for both the steam and CO_2 gasification reactions at the particle surface. Conditions for the experiment were shown earlier in Table 4. The measured mass release values (including replicates) of the Illinois #6 char when fed at the HPFFB steam/CO_2 conditions are shown in Figure 7, along with predictions of mass release by

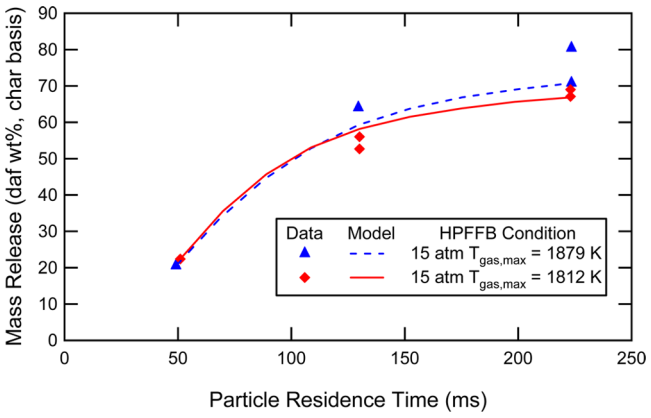

Figure 7. Measured and predicted values of daf mass release of 75−106 μm Illinois #6 coal char at the steam/CO_2 conditions in the HPFFB reactor at 15 atm.

the first-order model in eq 4. The predicted mass release curves in Figure 7 came from summing the particle mass release predicted by CO_2 and H_2O gasification using the first-order model in eq 4 and the Illinois #6 kinetic parameters in Table 8. The utilized kinetic parameters included published CO_2 parameters,[11] while the H_2O parameters were regressed in the current study from the data collected from the HPFFB steam conditions (see Table 3). The prediction of the particle mass release values approximated well the measured values at both conditions used in this study where the peak gas temperatures were 1812 and 1879 K. Although the partial pressure of CO_2 at the 15 atm $T_{gas,max}$ = 1812 K HPFFB condition was 2.5 times higher than that at the 15 atm $T_{gas,max}$ = 1879 K condition (see Table 4), similar mass release values were measured at both conditions (see Figure 7), since rates are exponential with temperature and the 15 atm $T_{gas,max}$ = 1879 K condition was hotter.

Parts a and b of Figure 8 show the predicted distribution of particle mass release caused by H_2O and CO_2 gasification when using the parameters in Table 8 in the first-order model for the case when the 75−106 μm Illinois #6 coal char was reinjected at the 15 atm $T_{gas,max}$ = 1812 K and 15 atm $T_{gas,max}$ = 1879 K steam/CO_2 HPFFB conditions, respectively. Although the first-order model predicted similar *total* mass release of Illinois #6 coal char at the two steam/CO_2 HPFFB conditions, it is predicted that 62% of the total particle mass release is due to CO_2 at the 15 atm $T_{gas,max}$ = 1812 K condition when compared to only 43% at the 15 atm $T_{gas,max}$ = 1879 K condition at particle residence times near 220 ms. The CO_2-induced mass release of Illinois #6 char at the two steam/CO_2 HPFFB conditions (see Figure 8) was higher when compared to the condition summarized in Figure 4 partly because the partial pressure of CO_2 at the 15 atm $T_{gas,max}$ = 1830 K steam condition was 2.4−6.1 times lower.

4. MODELING OF CHAR GASIFICATION DATA BY THE CCK MODELS

Two advanced models were also used to fit the measured char gasification data from the HPFFB reactor. These two models were the carbon conversion kinetic (CCK) model, and the CCK^N model which is an *n*th-order variant of the CCK model. These models as well as the multiple versions[49−51] of the carbon burnout kinetic (CBK)[31] model from which they stem are some of the most advanced char conversion models in the literature. The primary strength of these models is the ability to predict the experimentally observed loss of char reactivity at high conversions; the models primarily accomplish this by utilizing char deactivation submodels of thermal annealing and ash inhibition. Only certain aspects of the CCK and CCK^N models are included here, since both models have previously been described in great detail.[11,29] Note that the CCK model includes mechanisms to account for CO inhibition, but the data collected here are unfortunately inadequate to explore the inhibition in a meaningful way.

Both the CCK and CCK^N models utilized the random pore model[52−54] to account for surface area development in the reacting char. The empirical structural parameter, ψ, of the random pore model was typically fixed at a value of 4.6 in this study to be consistent with the work of others,[11,49] but the dimensionless ψ sometimes served as an adjustable parameter.

Both the CCK and CCK^N models utilized effectiveness factors[11,29,49−51,55,56] in their respective rate expressions to account for any pore-diffusion effects. The models both required the user to input a pore structure parameter, τ/f, which was used to calculate the effective diffusivity in the porous char, thereby influencing the effectiveness factor. The dimensionless parameter τ/f is defined as the tortuosity divided by the fraction of total porosity in the macropores.[11,49,51] In this study, τ/f was typically set to a value of 6 when modeling with the CCK^N model and a value of 12 when modeling with the CCK model to maintain consistency with variants of the CBK model.[11,50,51] However, τ/f sometimes served as an adjustable

DOI: 10.1021/ef502608y
Energy Fuels 2015, 29, 1479−1493

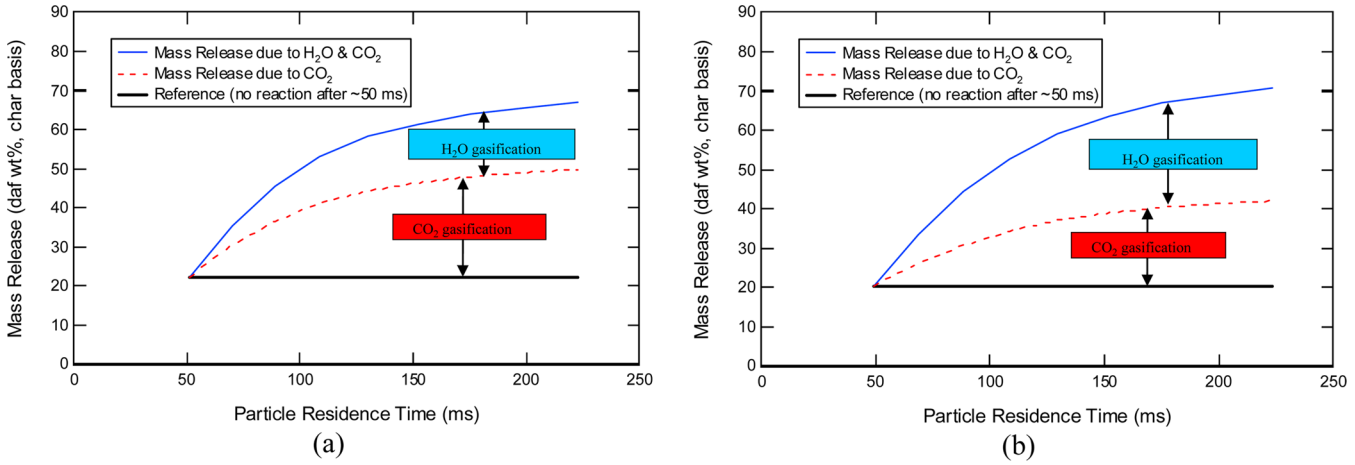

Figure 8. First-order model predictions for the distribution of particle mass release caused by H_2O and CO_2 gasification using kinetic parameters in Table 8 for Illinois #6 char gasified at 15 atm at the (a) $T_{gas,max}$ = 1812 K and (b) $T_{gas,max}$ = 1879 K steam/CO_2 HPFFB conditions.

Table 9. Optimized Parameters for Use in the CCK^N Model Using τ/f = 6 and ψ = 4.6 Unless Otherwise Noted

case identifier	optimized parameters	parameter names	ILL #6	Utah	Pitt #8
case #1	A_{H_2O}, E_{H_2O}, A_{CO_2}, E_{CO_2}	A_{H_2O} [$s^{-1}\cdot(mol/m^3)^n$], n = 0.5	1.49×10^7	2.01×10^7	3.78×10^7
		E_{H_2O} [kJ/mol]	168	168	168
		A_{CO_2} [$s^{-1}\cdot(mol/m^3)^n$], n = 0.5	3.13×10^6	6.47×10^6	1.25×10^6
		E_{CO_2} [kJ/mol]	151	153	185
		average absolute error[a]	8.2%	8.2%	8.1%
case #2	A_{H_2O}, A_{CO_2}	A_{H_2O} [$s^{-1}\cdot(mol/m^3)^n$], n = 0.5	4.48×10^6	6.25×10^6	6.56×10^6
		E_{H_2O} [kJ/mol]	168	168	168
		A_{CO_2} [$s^{-1}\cdot(mol/m^3)^n$], n = 0.5	1.09×10^6	1.39×10^6	1.09×10^6
		E_{CO_2} [kJ/mol]	146	146	146
		average absolute error[a]	9.4%	8.1%	8.5%
case #3	A_{H_2O}, A_{CO_2}, τ/f, ψ	A_{H_2O} [$s^{-1}\cdot(mol/m^3)^n$], n = 0.5	2.89×10^6	5.50×10^6	5.36×10^6
		E_{H_2O} [kJ/mol]	146	146	146
		A_{CO_2} [$s^{-1}\cdot(mol/m^3)^n$], n = 0.5	1.09×10^6	1.24×10^6	8.95×10^5
		E_{CO_2} [kJ/mol]	146	146	146
		τ/f	0.90	24.99	25
		ψ	10	7.28	10
		average absolute error[a]	8.5%	7.1%	7.7%

[a]Char basis.

parameter in this study, since Shurtz and Fletcher[11] identified it as a likely candidate to improve the model fit.

Similarly as was done when modeling the char gasification HPFFB data with the first-order model, data gathered from the first collection height at 25 mm above the burner served as reference data in the CCK and CCK^N models, since only the mass that was released from the particles after this first collection point was used in the modeling. This prevented the regressed kinetic parameters from being affected by any uncertainties in temperature history in the near-burner region.

Recall that only the Illinois #6 data measured at the HPFFB steam conditions (see Table 3) were used to regress Illinois #6 kinetic parameters for the global first-order model (see section 3.1), and that the regressed rate parameters were then used to predict the particle mass release of Illinois #6 char at the steam/CO_2 conditions (see Table 4 and section 3.3). However, all the measured Illinois #6 HPFFB data (i.e., from steam conditions and steam/CO_2 conditions) were used to regress kinetic parameters for both the CCK and CCK^N models.

4.1. Gasification Data Fit to the CCK^N Model. The CCK^N model was developed with many similarities to the char combustion model CBK8,[51] a widely used variant of the CBK model.[31] The CCK^N model utilized separate nth-order global rate expressions for the gasification of char by CO_2 and H_2O. Parameter optimization was performed by minimizing the sum squared error between measured and modeled particle mass release. Similar to the first-order model, the partial pressures of CO or H_2 were neglected in the optimization of CCK^N parameters, since the CCK^N model does not contain any inhibitory mechanisms. The reaction orders for the char/CO_2 and char/H_2O reactions were set to 0.5[7,11] to simplify parameter optimization. Gasification data from the 10 atm $T_{gas,max}$ = 1850 K nonsteam condition in the HPFFB (see section 2.4) were used to aid in the regression of the CO_2 rate parameters in the CCK^N model.

The fitting parameters included the activation energies and the pre-exponential factors for the char/CO_2 and char/H_2O reactions, in addition to the random pore model parameter (ψ)

DOI: 10.1021/ef502608y
Energy Fuels 2015, 29, 1479−1493

and the pore structure parameter (τ/f) (see case #3 in Table 9). Optimization case #1 was performed by allowing both activation energies and pre-exponential factors to vary, but it was found that the fit only worsened slightly when only pre-exponential factors were allowed to vary while CO_2 and H_2O activation energies were kept constant at 146 kJ/mol (case #2). The last optimization case #3 allowed both CO_2 and H_2O pre-exponential factors to vary, in addition to ψ and τ/f. For all of the optimizations, the values of the activation energies were highly correlated with the pre-exponential factor. There was quite a range of activation energies (with associated pre-exponential factors) that would fit these data. The activation energies and associated pre-exponential factors presented in this paper fit the data but are therefore not considered unique. It follows that these activation energies should not be used to infer the regime of char combustion (e.g., if pore diffusion controls).

Table 9 shows the results of the three optimized cases from the CCK^N model, and Figure 9 is a parity plot of the

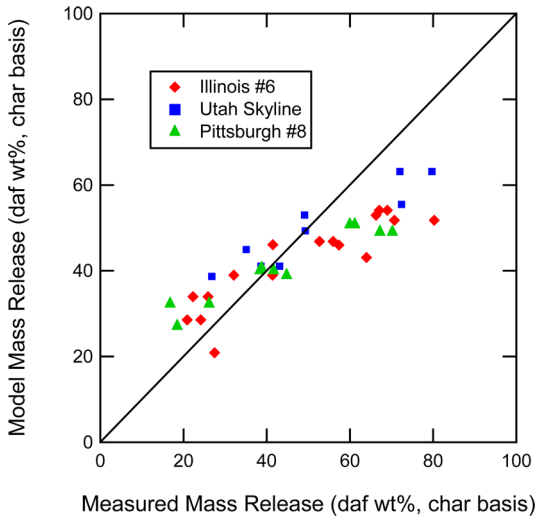

Figure 9. Fit of char mass release HPFFB data with the CCK^N model for the optimized case #3 (A_{H_2O}, A_{CO_2}, τ/f, and ψ as fitting parameters).

predictions of particle conversions vs the measured HPFFB data for the optimized case #3. The average absolute errors are reported in Table 9, and the errors of 7−9% for all three cases are encouraging. It must be noted that the kinetic parameters in Table 9 are influenced by the annealing and ash inhibition submodels, which means that the reported rate parameters should only be used in models that contain all the same features as the CCK^N model. Note the slight skew in Figure 9 where the model initially overpredicts char conversion while underpredicting conversion at late burnout. Shurtz and Fletcher[11] observed a similar skew when fitting coal CO_2 gasification data to the CCK^N model. A possible explanation for the skew in Figure 9 is that the thermal annealing and ash inhibition submodels contained in the CCK^N model overpredict the char deactivation effect for coal gasification rates at the conditions used in the current study.

In addition to the χ factor, the η value (effectiveness factor) derived from the Thiele modulus indicates the relative importance of kinetic and pore diffusion resistances. In these experiments, η ranged from about 0.8 to 1 (rising toward the kinetic limit of 1 as char annealing proceeded), consistent with the χ factor. This indicates an initial zone II regime where both kinetic and pore diffusion limit the reaction, and shows that the reaction proceeds toward zone I as the char conversion and annealing progress.

A parameter sensitivity analysis of the CCK^N model was performed by examining how predicted char conversion was influenced by the user-defined parameters ψ and τ/f for Illinois #6 char gasified at the 10 atm $T_{gas,max}$ = 1814 K HPFFB steam condition (see Table 3). Figure 10 shows the results of this

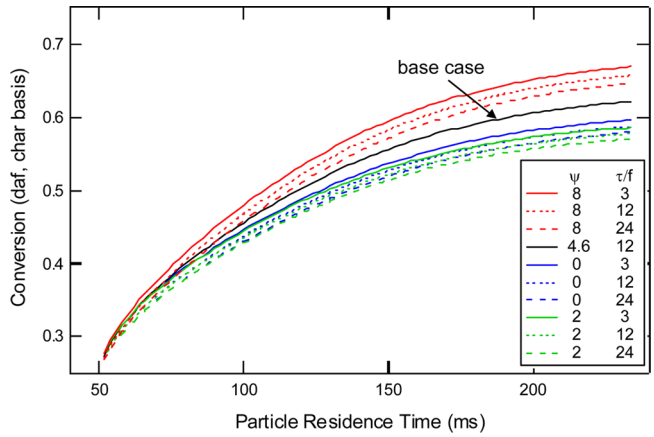

Figure 10. Effect of ψ and τ/f on Illinois #6 char conversion at the 10 atm $T_{gas,max}$ = 1814 K HPFFB steam condition when using the CCK^N model.

analysis, and it is seen that both τ/f and ψ parameters in the CCK model significantly influenced the char conversion predictions. As discussed by Shurtz,[29] a higher τ/f indicates either higher macropore tortuosity or a higher fraction of pore volume in micro- and mesopores, while a higher value of ψ indicates that char gasification significantly affects pore structure. This sensitivity analysis showed that ψ was the more sensitive parameter, contrary to the findings of Shurtz,[29] although this study differed from that of Shurtz in several respects including coal type, gasification temperature, and the inclusion of H_2O gasification data.

4.2. Gasification Data Fit to the CCK Model. The CCK model was adapted by Shurtz[11,29] and is a combination of the CBK/E[50] and CBK/G[49] models. The CCK model was the most complicated of the three models used to fit the measured HPFFB data in this work. The Langmuir−Hinshelwood kinetics in the CCK code models combustion and gasification of char using a three-step combustion mechanism and a five-step gasification mechanism, as shown in Table 10, where C(O) is the oxide complex on the char surface. As in the CBK/G[49] model, gasification reaction rate constants were scaled to one of the individual steps to simplify the optimization of rate parameters. This allowed the multistep kinetic model in the CCK code to be fit to measured HPFFB gasification data by

Table 10. Char Conversion Eight-Step Mechanism in the CCK Model

combustion	gasification
$2C + O_2 \rightarrow C(O) + CO$	$C + CO_2 \leftrightarrow C(O) + CO$
$C + C(O) + O_2 \rightarrow CO_2 + C(O)$	$C(O) \rightarrow CO$
$C(O) \rightarrow CO$	$C + H_2O \leftrightarrow C(O) + H_2$
	$C(O) \rightarrow CO$
	$C + 2H_2 \rightarrow CH_4$

DOI: 10.1021/ef502608y
Energy Fuels 2015, 29, 1479−1493

Table 11. Optimized Parameters for Use in the CCK Model Using τ/f = 12 and ψ = 4.6 Unless Otherwise Noted

case identifier	optimized parameters	parameter names	ILL #6	Utah	Pitt #8
case #1	A_7, E_7	A_7 [s^{-1}]	3.31×10^7	9.97×10^8	9.76×10^8
		E_7 [kJ/mol]	121	166	166
		average absolute error[a]	13.2%	8.6%	9.2%
case #2	A_7	A_7 [s^{-1}]	2.10×10^8	2.45×10^8	2.31×10^8
		E_7 [kJ/mol]	146	146	146
		average absolute error[a]	12.7%	8.8%	9.4%
case #3	A_7, τ/f, ψ	A_7 [s^{-1}]	1.76×10^8	2.14×10^8	2.04×10^8
		E_7 [kJ/mol]	146	146	146
		τ/f	13.81	25	25
		ψ	10	10	10
		average absolute error[a]	12.5%	8.1%	8.9%

[a]Char basis.

varying a single set of Arrhenius rate parameters. The partial pressures of CO_2, H_2O, CO, and H_2 in the postflame HPFFB environment were input for each condition when modeling with the CCK code.

Parameter optimization was performed by minimizing the sum squared error between measured and modeled particle mass release. Optimization case #1 was performed by allowing A_7 and E_7 to vary (pre-exponential factor and activation energy of the seventh step of the gasification scaling reaction), but it was found that the average absolute error only changed by less than 4% when A_7 was allowed to vary while E_7 was kept constant at 168 kJ/mol (case #2). The last optimization case #3 allowed A_7, ψ, and τ/f to vary, and the absolute error decreased by up to 9%.

Table 11 contains the results of the three optimized cases from the CCK model, while Figure 11 is a parity plot of particle

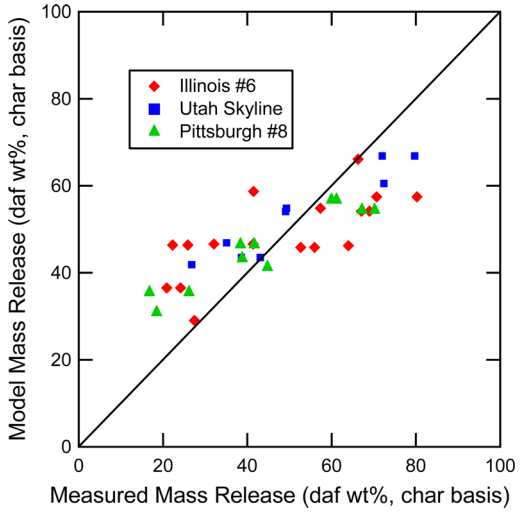

Figure 11. Fit of char mass release HPFFB data with the CCK model for the optimized case #3 (A_7, τ/f, and ψ as fitting parameters).

conversion predictions vs the measured HPFFB data for the optimized case #3. The low absolute errors for the three optimized CCK cases reported in Table 11 are encouraging, and the fits of the gasification HPFFB data by the CCK^N and CCK models were comparable to each other. Note that the kinetic parameters in Table 11 are influenced by the annealing and ash inhibition submodels contained in the CCK model, so accurate predictions would only be expected when the reported parameters are used in a model containing all the same features as the CCK model. Similar to Figure 9, a slight skew exists in Figure 11 where the CCK model initially overpredicts char conversion and underpredicts particle mass release at high conversions. Again, the skew could perhaps be explained by the overpredicted effect of char deactivation at the experimental conditions used in this study by the thermal annealing and ash inhibition submodels in the CCK model.

A parameter sensitivity analysis of the CCK model was performed to examine how the user-defined parameters ψ and τ/f influenced the predicted char conversion. As discussed above, the optimized values of τ/f and ψ from case #3 improved the fit with a decrease in average absolute error up to 9%. Figure 12 shows a simple sensitivity analysis of Illinois #6 char

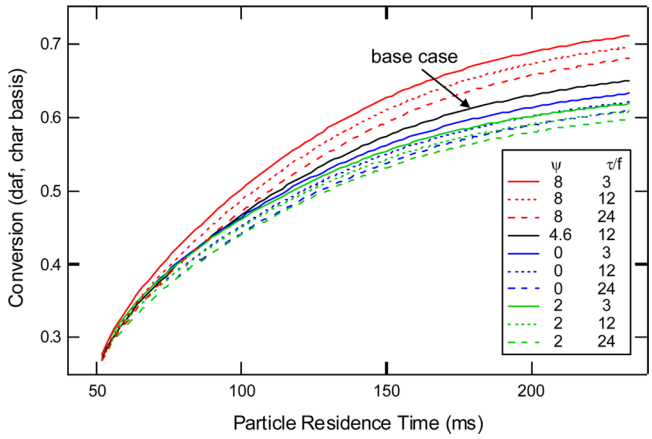

Figure 12. Effect of ψ and τ/f on Illinois #6 char conversion at the 10 atm $T_{gas,max}$ = 1814 K HPFFB steam condition using the CCK model.

gasified at the 10 atm $T_{gas,max}$ =1814 K steam HPFFB condition (see Table 3). Similarly to the case with the CCK^N model, it is seen in Figure 12 that predictions of char conversion by the CCK model are influenced significantly by both τ/f and ψ parameters.

Note also that the case #3 optimizations (see Tables 9 and 11) often pushed ψ and τ/f to the edges of their allowed bounds in the constrained optimizations. This implies that, while both are sensitive parameters, the reported values of ψ and τ/f do not maintain their physical meaning but rather are compensating for other factors not captured in the models. The fits and predictive power of both the CCK^N and CCK models could be improved by increasing the accuracy of their submodels, including the utilization of more physically

DOI: 10.1021/ef502608y
Energy Fuels 2015, 29, 1479−1493

meaningful values of ψ and τ/f. These improvements will be the focus of future research.

5. SUMMARY AND CONCLUSIONS

Pulverized coal chars were generated in a pressurized flat-flame burner apparatus (HPFFB) at temperatures up to 1830 K, pressures up to 15 atm, and particle heating rates of 10^5 K/s. These heating conditions are closer to the conditions encountered in industrial entrained flow gasifiers than has been possible before in pressurized drop tube experiments. In particular, the swelling characteristics and reactivity have been shown previously[30,57−59] to be influenced by changing the particle heating rate from 10^4 K/s (as in drop tube reactors) to 10^5 K/s (as in FFB experiments). Chars were sieved and reinjected into the HPFFB to obtain steam-char gasification rates at the same pressures, heating rates, and temperatures at which the chars were generated. Most of the experiments were performed at conditions where the majority of particle mass release was due to H_2O gasification, although some experiments were performed using Illinois #6 char at conditions where significant mass release was due to gasification by both H_2O and CO_2. Steam gasification rates of three bituminous coal chars (Illinois #6, Utah Skyline, and Pittsburgh #8) were modeled using measured data from the entrained-flow HPFFB reactor. Three different char gasification models were used to fit the data, including a first-order global model and the more complex CCK^N and CCK models.

When modeling the char gasification data from the HPFFB steam conditions with the first-order model, the low CO_2-induced char conversion was taken into account and the remaining measured particle mass release was attributed to H_2O gasification. The particle mass release data caused by H_2O were then used to regress H_2O gasification kinetic parameters for the global first-order model. Pittsburgh #8 char was measured to be 2.3 times more reactive to steam than the Illinois #6 char and 1.6 times more reactive to steam than the Utah Skyline char. Steam gasification rates were measured to be 6−16 times faster than CO_2 gasification rates at the conditions studied. The total particle mass release measured from Illinois #6 char (75−106 μm) reacting at the steam/CO_2 HPPFB conditions was accurately predicted by summing the particle mass release predicted by CO_2 and H_2O gasification using the first-order kinetic parameters documented in this work. All the HPFFB char gasification data were shown to have reacted far below the film-diffusion limit.

The HPFFB char gasification data were also fit to the advanced CCK^N and CCK models that treat the experimentally observed decrease in char reactivity at high conversions using char deactivation submodels of thermal annealing and ash inhibition. Rate parameters for these models were reported, although some caution is warranted in their use, since they were influenced by the specific submodels contained in the CCK^N and CCK codes. Char deactivation may have been overpredicted by the submodels of the CCK^N and CCK codes at the experimental conditions used in this study. From the limited conditions explored in this study, predictions of char conversion by both the CCK^N and CCK models were influenced more by the user-defined ψ parameter than by τ/f. The fits of the HPFFB gasification data by the CCK^N and CCK models were comparable to each other.

AUTHOR INFORMATION

Corresponding Author

*Address: Chemical Engineering Department, 350 CB, Brigham Young University, Provo, UT 84602. E-mail: tom_fletcher@byu.edu.

Notes

Disclosure: The views and opinions of authors expressed herein do not necessarily state or reflect those of the United States Government or any agency thereof.

The authors declare no competing financial interest.

ACKNOWLEDGMENTS

This material is based upon work supported by the Department of Energy under Award Number DE-NT0005015 and partially by the Department of Energy, National Nuclear Security Administration, under Award Number(s) DE-NA0002375.

REFERENCES

(1) NETL National energy technology laboratory gasification worldwide database, http://www.Netl.Doe.Gov/research/coal/energy-systems/gasification/gasification-plant-databases. http://www.netl.doe.gov/research/coal/energy-systems/gasification/gasification-plant-databases/2010-archive 2010 (Last accessed Feb 25, 2014).

(2) Liu, K.; Cui, Z.; Fletcher, T. H. Coal gasification. In *Hydrogen and Syngas Production and Purification Technologies*; Liu, K., Song, C., Subramani, V., Eds.; John Wiley & Sons: Hoboken, NJ, 2010; pp 156−218.

(3) Minchener, A. J. Coal gasification for advanced power generation. *Fuel* **2005**, *84* (17), 2222−2235.

(4) Ren, L. W.; Yang, J. L.; Gao, F.; Yan, J. D. Laboratory study on gasification reactivity of coals and petcokes in co2/steam at high temperatures. *Energy Fuels* **2013**, *27* (9), 5054−5068.

(5) Essenhigh, R. H. Fundamentals of coal combustion. In *Chemistry of Coal Utilization*, 2nd suppl. vol.; Elliot, M. A., Ed.; John Wiley & Sons Inc.: New York, 1981; Chapter 19.

(6) Fletcher, T. H.; Ma, J. L.; Rigby, J. R.; Brown, A. L.; Webb, B. W. Soot in coal combustion systems. *Prog. Energy Combust. Sci.* **1997**, *23* (3), 283−301.

(7) Fermoso, J.; Gil, M. V.; Garcia, S.; Pevida, C.; Pis, J. J.; Rubiera, F. Kinetic parameters and reactivity for the steam gasification of coal chars obtained under different pyrolysis temperatures and pressures. *Energy Fuels* **2011**, *25* (8), 3574−3580.

(8) Roberts, D. G.; Harris, D. J.; Wall, T. F. On the effects of high pressure and heating rate during coal pyrolysis on char gasification reactivity. *Energy Fuels* **2003**, *17* (4), 887−895.

(9) Wu, Y. Q.; Wu, S. Y.; Gu, J.; Gao, J. S. Differences in physical properties and co$_2$ gasification reactivity between coal char and petroleum coke. *Process Saf. Environ. Prot.* **2009**, *87* (5), 323−330.

(10) Wu, S.; Gu, J.; Li, L.; Wu, Y.; Gao, J. The reactivity and kinetics of Yanzhou coal chars from elevated pyrolysis temperatures during gasification in steam at 900−1200 °C. *Process Saf. Environ. Prot.* **2006**, *84* (6), 420−428.

(11) Shurtz, R. C.; Fletcher, T. H. Coal char-CO_2 gasification measurements and modeling in a pressurized flat-flame burner. *Energy Fuels* **2013**, *27* (6), 3022−3038.

(12) Wall, T. F.; Liu, G. S.; Wu, H. W.; Roberts, D. G.; Benfell, K. E.; Gupta, S.; Lucas, J. A.; Harris, D. J. The effects of pressure on coal reactions during pulverised coal combustion and gasification. *Prog. Energy Combust. Sci.* **2002**, *28* (5), 405−433.

(13) Weeda, M.; Abcouwer, H. H.; Kapteijn, F.; Moulijn, J. A. Steam gasification kinetics and burn-off behavior for a bituminous coal-derived char in the presence of h-2. *Fuel Process. Technol.* **1993**, *36* (1−3), 235−242.

(14) Ahn, D. H.; Gibbs, B. M.; Ko, K. H.; Kim, J. J. Gasification kinetics of an indonesian sub-bituminous coal-char with CO2 at elevated pressure. *Fuel* **2001**, *80* (11), 1651−1658.

DOI: 10.1021/ef502608y
Energy Fuels 2015, 29, 1479−1493

(15) Kajitani, S.; Hara, S.; Matsuda, H. Gasification rate analysis of coal char with a pressurized drop tube furnace. *Fuel* **2002**, *81* (5), 539−546.
(16) Kajitani, S.; Suzuki, N.; Ashizawa, M.; Hara, S. CO_2 gasification rate analysis of coal char in entrained flow coal gasifier. *Fuel* **2006**, *85* (2), 163−169.
(17) Fermoso, J.; Gil, M. V.; Pevida, C.; Pis, J. J.; Rubiera, F. Kinetic models comparison for non-isothermal steam gasification of coal-biomass blend chars. *Chem. Eng. J.* **2010**, *161* (1−2), 276−284.
(18) Huang, Z. M.; Zhang, J. S.; Zhao, Y.; Zhang, H.; Yue, G. X.; Suda, T.; Narukawa, M. Kinetic studies of char gasification by steam and CO_2 in the presence of h-2 and co. *Fuel Process. Technol.* **2010**, *91* (8), 843−847.
(19) Liu, H.; Zhu, H.; Kaneko, M.; Kato, S.; Kojima, T. High-temperature gasification reactivity with steam of coal chars derived under various pyrolysis conditions in a fluidized bed. *Energy Fuels* **2010**, *24*, 68−75.
(20) Xu, Q. X.; Pang, S. S.; Levi, T. Reaction kinetics and producer gas compositions of steam gasification of coal and biomass blend chars, part 1: Experimental investigation. *Chem. Eng. Sci.* **2011**, *66* (10), 2141−2148.
(21) Li, F.; Li, X. H.; Yao, R. S.; Chang, L. P.; Zhang, Q. G. A kinetics study on the gasification of poor quality coal. *Energy Sources, Part A* **2012**, *34* (21), 1943−1957.
(22) Fan, D. M.; Zhu, Z. P.; Na, Y. J.; Lu, Q. G. Thermogravimetric analysis of gasification reactivity of coal chars with steam and CO_2 at moderate temperatures. *J. Therm. Anal. Calorim.* **2013**, *113* (2), 599−607.
(23) Tremel, A.; Spliethoff, H. Gasification kinetics during entrained flow gasification - part ii: Intrinsic char reaction rate and surface area development. *Fuel* **2013**, *107*, 653−661.
(24) Huo, W.; Zhou, Z. J.; Wang, F. C.; Wang, Y. F.; Yu, G. S. Experimental study of pore diffusion effect on char gasification with CO_2 and steam. *Fuel* **2014**, *131*, 59−65.
(25) Yan, Q. X.; Huang, J. J.; Zhao, J. T.; Li, C. Y.; Xia, L. S.; Fang, Y. T. Investigation into the kinetics of pressurized steam gasification of chars with different coal ranks. *J. Therm. Anal. Calorim.* **2014**, *116* (1), 519−527.
(26) Bai, Y. H.; Wang, Y. L.; Zhu, S. H.; Yan, L. J.; Li, F.; Xie, K. C. Synergistic effect between CO_2 and H_2O on reactivity during coal chars gasification. *Fuel* **2014**, *126*, 1−7.
(27) Lewis, A. Gasification of biomass, coal, and petroleum coke at high heating rates and elevated pressure. Ph.D. Dissertation, Chemical Engineering, Brigham Young University, Provo, UT, 2014. http://www.et.byu.edu/~tom/Papers/Aaron_Lewis_Dissertation%28FINAL%29.pdf (last accessed Feb 16, 2015).
(28) Lewis, A. D. Sawdust pyrolysis and petroleum coke CO_2 gasification at high heating rates. M.S. Thesis, Chemical Engineering, Brigham Young University, Provo, UT, 2011. http://scholarsarchive.byu.edu/etd/2498/ (last accessed Feb 16, 2015).
(29) Shurtz, R. Effects of pressure on the properties of coal char under gasification conditions at high initial heating rates. Ph.D. Dissertation, Chemical Engineering, Brigham Young University, 2011. http://scholarsarchive.byu.edu/etd/2877/ (last accessed Feb 16, 2015).
(30) Shurtz, R. C.; Hogge, J. W.; Fowers, K. C.; Sorensen, G. S.; Fletcher, T. H. Coal swelling model for pressurized high particle heating rate pyrolysis applications. *Energy Fuels* **2012**, *26* (6), 3612−3627.
(31) Hurt, R.; Sun, J. K.; Lunden, M. A kinetic model of carbon burnout in pulverized coal combustion. *Combust. Flame* **1998**, *113* (1−2), 181−197.
(32) Hecht, E. S.; Lighty, J. S.; Shaddix, C. R. *Kinetic rates of oxidation and gasification reactions of coal chars reacting in oxy-combustion environments*, presented at the 8th U.S. National Combustion Meeting, Park City, UT, May 19−22, 2013.
(33) Shurtz, R. C.; Kolste, K. K.; Fletcher, T. H. Coal swelling model for high heating rate pyrolysis applications. *Energy Fuels* **2011**, *25* (5), 2163−2173.
(34) Lewis, A. D.; Fletcher, E. G.; Fletcher, T. H. CO_2 gasification rates of petroleum coke in a pressurized flat-flame burner entrained-flow reactor. *Energy Fuels* **2014**, *28*, 4447−4457.
(35) Goetz, G. J.; Nsakala, N. Y.; Patel, R. L.; Lao, T. C. *Combustion and gasification kinetics of chars from four commercially significant coals of varying rank*, presented at the Second Annual Contractors' Conference on Coal Gasification, Palo Alto, CA, 1982.
(36) Lewis, A. D.; Fletcher, E. G.; Fletcher, T. H. CO_2 char gasification rates of sawdust, switchgrass, and corn stover in a pressurized entrained-flow reactor. *Energy Fuels* **2014**, *28*, 5812−5825.
(37) Sowa, J. M. Studies of coal nitrogen release chemistry for oxyfuel combustion and chemical additives. M.S. Thesis, Chemical Engineering, Brigham Young University, 2009.
(38) Turkdogan, E. T.; Vinters, J. V. Effect of carbon monoxide on the rate of oxidation of charcoal, graphite and coke in carbon dioxide. *Carbon* **1970**, *8*, 39−53.
(39) Guizani, C.; Sanz, F. J. E.; Salvador, S. The gasification reactivity of high-heating-rate chars in single and mixed atmospheres of H_2O and CO_2. *Fuel* **2013**, *108*, 812−823.
(40) Roberts, D. G.; Harris, D. J. Char gasification in mixtures of CO_2 and H_2O: Competition and inhibition. *Fuel* **2007**, *86* (17−18), 2672−2678.
(41) Smith, I. W. *The combustion rates of coal chars: A review*, presented at the Nineteenth Internal Symposium on Combustion, Pittsburgh, PA, 1982.
(42) Smith, K. L.; Smoot, L. D.; Fletcher, T. H.; Pugmire, R. J. *The structure and reaction processes of coal*. Plenum Press: New York, 1994.
(43) Smoot, L. D.; Smith, P. J. *Coal combustion and gasification*; Plenum Press: New York, 1985.
(44) Everson, R. C.; Neomagus, H.; Kasaini, H.; Njapha, D. Reaction kinetics of pulverized coal-chars derived from inertinite-rich coal discards: Gasification with carbon dioxide and steam. *Fuel* **2006**, *85* (7−8), 1076−1082.
(45) Walker, P. L.; Rusinko, F. J.; Austin, L. G. Gas reactions of carbon. *Adv. Catal.* **1959**, *11*, 133−221.
(46) Zhang, R.; Wang, Q. H.; Luo, Z. Y.; Fang, M. X.; Cen, K. F. Competition and inhibition effects during coal char gasification in the mixture of H_2O and CO_2. *Energy Fuels* **2013**, *27* (9), 5107−5115.
(47) Ahmed, I. I.; Gupta, A. K. Kinetics of woodchips char gasification with steam and carbon dioxide. *Appl. Energy* **2011**, *88* (5), 1613−1619.
(48) Moilanen, A.; Muhlen, H. J. Characterization of gasification reactivity of peat char in pressurized conditions - effect of product gas inhibition and inorganic material. *Fuel* **1996**, *75* (11), 1279−1285.
(49) Liu, G. S.; Niksa, S. Coal conversion submodels for design applications at elevated pressures. Part ii. Char gasification. *Prog. Energy Combust. Sci.* **2004**, *30* (6), 679−717.
(50) Niksa, S.; Liu, G. S.; Hurt, R. H. Coal conversion submodels for design applications at elevated pressures. Part i. Devolatilization and char oxidation. *Prog. Energy Combust. Sci.* **2003**, *29* (5), 425−477.
(51) Sun, J. K.; Hurt, R. H. Mechanisms of extinction and near-extinction in pulverized solid fuel combustion. *Proc. Combust. Inst.* **2000**, *28*, 2205−2213.
(52) Bhatia, S. K.; Perlmutter, D. D. A random pore model for fluid-solid reactions 0.1. Isothermal, kinetic control. *AIChE J.* **1980**, *26* (3), 379−386.
(53) Bhatia, S. K.; Perlmutter, D. D. A random pore model for fluid-solid reactions. 2. Diffusion and transport effects. *AIChE J.* **1981**, *27* (2), 247−254.
(54) Gavalas, G. R. A random capillary model with application to char gasification at chemically controlled rates. *AIChE J.* **1980**, *26* (4), 577−585.
(55) Bischoff, K. B. Effectiveness factors for general reaction rate forms. *AIChE J.* **1965**, *11* (2), 351−355.
(56) Carberry, J. J. The micro-macro effectiveness factor for the reversible catalytic reaction. *AIChE J.* **1962**, *8* (4), 557−558.
(57) Gale, T. K.; Bartholomew, C. H.; Fletcher, T. H. Decreases in the swelling and porosity of bituminous coals during devolatilization at high heating rates. *Combust. Flame* **1995**, *100* (1−2), 94−100.

DOI: 10.1021/ef502608y
Energy Fuels 2015, 29, 1479−1493

(58) Gale, T. K.; Bartholomew, C. H.; Fletcher, T. H. Effects of pyrolysis heating rate on intrinsic reactivities of coal chars. *Energy Fuels* **1996**, *10* (3), 766−775.
(59) Gale, T. K.; Fletcher, T. H.; Bartholomew, C. H. Effects of pyrolysis conditions on internal surface areas and densities of coal chars prepared at high heating rates in reactive and nonreactive atmospheres. *Energy Fuels* **1995**, *9* (3), 513−524.

DOI: 10.1021/ef502608y
Energy Fuels 2015, 29, 1479−1493